Journal of the Meteorological Society of Japan, Vol. 96, No. 2, pp. 111−126, 2018
DOI:10.2151/jmsj.2018-014

Effect of the Initial Vortex Structure on Intensification of a Numerically Simulated Tropical Cyclone

Jing XU

State Key Laboratory of Severe Weather, Chinese Academy of Meteorological Sciences, China Meteorological Administration, China

and

Yuqing WANG

State Key Laboratory of Severe Weather, Chinese Academy of Meteorological Sciences, China Meteorological Administration, China
Department of Atmospheric Sciences and International Pacific Research Center, University of Hawaii at Manoa, Hawaii, USA

(Manuscript received 18 July 2017, in final form 13 December 2017)

Abstract

The dependence of the intensification rate (IR) of a tropical cyclone (TC) on its initial structure, including the radius of maximum wind (RMW) and the radial decay rate of tangential wind outside the RMW, is examined based on ensemble of simulations using a nonhydrostatic axisymmetric cloud-resolving model. It is shown that the initial spinup period is shorter, and the subsequent IR is larger for a storm with an initially smaller RMW or with an initially more rapid radial decay of tangential wind outside the RMW. The results show that the longevity of the initial spinup period is determined by how quickly the inner-core region becomes nearly saturated in the middle and lower troposphere, and thus, deep convection near the RMW is initiated and organized. Because of the larger volume and weaker Ekman pumping, the inner core of the initially larger vortex takes longer time to become saturated and thus experiences a longer initial spinup period. The vortex initially with the larger RMW (with the slower radial decay of tangential wind outside the RMW) has lower inertial stability inside the RMW (higher inertial stability outside the RMW), develops more active convection in the outer-core region and weaker boundary-layer inflow in the inner-core region, and thus experiences lower IR during the primary intensification stage.

Keywords Tropical cyclone structure; Intensification rate

1. Introduction

Observational studies have shown that individual tropical cyclones (TCs) can have different radial structures, most prominently the radius of maximum wind (RMW) and the decay rate of the tangential wind with radius outside the RMW, even for TCs with similar intensities measured by maximum sustained 10-m wind speed (Merrill 1984; Weatherford and Gray 1988). It is generally believed that a variety of environmental conditions, such as vertical wind shear, relative humidity, and background vorticity, are responsible for the differences in the initial structure of a TC vortex when it forms over tropical oceans as well as the subsequent structural change from both

Corresponding author: Yuqing Wang, IPRC/SOEST, POST 404A, 1680 East-West Road, Honolulu, HI 96822, USA
E-mail: yuqing@hawaii.edu
J-stage Advance Published Date: 26 December 2017

©The Author(s) 2018. This is an open access article published by the Meteorological Society of Japan under a Creative Commons Attribution 4.0 International (CC BY 4.0) license (http://creativecommons.org/license/by/4.0).

observational and theoretical studies (Knaff 2004; Xu and Wang 2010a; Hill and Lackmann 2009). After its formation, a TC often experiences an intensification phase before it reaches its mature stage. During the intensification, the structure of a TC may be affected by both internal dynamical/physical processes and the complex external interactions between the storm and its environment, such as with the vertical wind shear (Wang and Wu 2004; Elsberry et al. 2013; Wang and Wang 2014). In turn, the TC intensification rate (IR) may be considerably affected by the structure of the TC vortex as well (Schubert and Hack 1982; Pendergrass and Willoughby 2009; Rogers 2010; Rogers et al. 2013).

Recent observational studies have shown that the TC IR is highly correlated with the TC structure, particularly its inner- and outer-core sizes (Chen et al. 2011; Rogers et al. 2013; Carrasco et al. 2014; Xu and Wang 2015). On the basis of the 20-year TC best track data in the North Atlantic, Carrasco et al. (2014) compared the rapid intensification (RI) and non-RI TC cases. They found that the RI TCs are more likely to have a smaller size in terms of the RMW, the average radius of 34-knot wind (AR34). In addition to the TC size, another TC structure parameter is the decay rate of tangential wind with radius outside the RMW. Rogers et al. (2013) compared the composite structures of intensifying and quasi-steady TCs based on airborne-radar data for North Atlantic TCs. They found that the tangential wind outside the RMW decays more rapidly with radius, and the eyewall heating is located more to the inside of the RMW, in intensifying TCs than in the quasi-steady TCs. Similar results were reported by Xu and Wang (2015) based on best-track data for North Atlantic TCs from 1980 to 2012; they measured the decay rate of tangential wind with radius outside the RMW as the width of the ring between the RMW and AR34 of a TC, which is referred to as the wind-skirt parameter (DR34). Xu and Wang (2015) also found that RI tends to occur in a relatively narrow parameter space in both inner- and outer-core sizes, with the highest IR occurring at an RMW of around 40 km and AR34 and DR34 of around 150 km. TCs intensify more frequently for an RMW between 20 and 60 km, an AR34 of about 200 km, and a DR34 of about 150 km (see Figs. 3, 4 in Xu and Wang 2015). These observational studies strongly suggest that TC IR depends on both the RMW and the decay rate of tangential wind outside the RMW.

Previous studies based on the axisymmetric balanced dynamics have argued for the importance of the inner-core inertial stability (Schubert and Hack 1982; Pendergrass and Willoughby 2009) and the radial location of eyewall heating relative to the RMW to the IR of TCs (Vigh and Schubert 2009). The IR is shown to be a function of the inertial stability in the inner core, which determines the efficiency of the warming in the eye and the tangential wind tendency in response to diabatic heating in the eyewall (Schubert and Hack 1982). Studies have demonstrated that the IR depends on both the radial location of diabatic heating relative to the RMW and the radial distribution of inertial stability (Vigh and Schubert 2009; Pendergrass and Willoughby 2009). In general, diabatic heating inside the RMW where the inertial stability is much higher than outside the RMW favors the formation of a warm core and larger IR (Vigh and Schubert 2009), and relatively higher inertial stability outside the RMW, related to the slow decay of the tangential wind outside the RMW, is unfavorable for large IR (Pendergrass and Willoughby 2009).

The above-cited results based on balanced dynamics have often been used to explain the dependence of IR on the inner-core structure of TCs in observations (Rogers et al. 2013; Carrasco et al. 2014; Xu and Wang 2015). Rogers et al. (2013) found that intensifying TCs have a stronger axisymmetric eyewall upward motion with more convective bursts located more on the inside of the RMW and a faster decay with radius of the tangential wind (and thus smaller relative vorticity and lower inertial stability) outside the RMW than steady-state TCs. Xu and Wang (2015) also attributed their observed dependence of TC IR on the outer-core wind skirt to the inertial stability outside the RMW, since the outer-core wind-skirt parameter DR34 reflects the radial decay rate of the tangential wind outside the RMW. In addition to the inertial stability, Wang and Xu (2010) and Xu and Wang (2010b) showed that the surface entropy flux within about 2–2.5 times of the RMW contributes to TC intensity, and the surface entropy flux farther outward contributes greatly to the growth of the storm inner- and outer-core sizes which could reduce TC intensity because of the development of active outer spiral rainbands (Wang 2009).

In this study, the nonhydrostatic, axisymmetric, full-physics model CM1 developed by Bryan and Fritsch (2002) was used to perform several ensemble simulations under idealized conditions to further understand the effect of the initial vortex structure on the initial spinup and the subsequent IR of the simulated TCs. The rest of the paper is organized as follows. Section 2 describes the numerical model and experimental design. Section 3 discusses the model

results and the possible physical mechanisms. The main conclusions are drawn in the last section.

2. Model and experimental design

The axisymmetric, nonhydrostatic cloud model version 1 (CM1, release 17) developed by Bryan and Fritsch (2002) was used to perform a series of numerical experiments in this study. CM1 has previously been used to understand various aspects of TCs, such as the maximum potential intensity (MPI) of TCs (Bryan and Rotunno 2009a, b), the sensitivities of TC MPI to the surface-exchange coefficient, and the turbulence mixing-length scale (Bryan 2012). A full description of CM1 can be found in Bryan and Rotunno (2009a, b). The model domain used in our simulations is 1500 km in radial direction with radial grid spacing of 1 km for $r < 188$ km and a stretched radial resolution for $r \geq 188$ km. There are 59 vertical levels, with the lowest model level at 25 m above the surface and the highest model level at the model top at 25 km. The vertical grid length varied from 50 to 430 m for $z < 5$ km in order to better resolve boundary-layer processes and was 500 m for $z \geq 5$ km. The use of an axisymmetric numerical model allows for a large number of ensemble simulations at relatively low computational cost.

The radial profile of tangential wind of the initial vortices is given by

$$V(r,z)=\begin{cases} V_m(z)\dfrac{r}{r_m}, & r \leq r_m \\ V_m(z)\dfrac{r}{r_m}\exp\left\{\dfrac{1}{B}\left[1.0-\left(\dfrac{r}{r_m}\right)^B\right]\right\} \\ \quad -\dfrac{r-r_m}{r_0-r_m}\exp\left\{\dfrac{1}{B}\left[1.0-\left(\dfrac{r_0}{r_m}\right)^B\right]\right\}, & r > r_m \end{cases} \tag{1}$$

where r_m is the RMW, $V_m(z)$ is the maximum tangential wind speed, which takes its maximum value near the surface and decreases linearly with height to zero at 100 hPa, z is height, r is the radius from the TC center, r_0 is the radius beyond which the tangential wind vanishes, and the parameter B is the factor that defines the decay rate of tangential wind with radius outside the RMW and thus determines the outer-core shape of the initial vortex. Large (small) B represents rapid (slow) radial decay of tangential wind outside the RMW. Note that the initial tangential wind inside the RMW is assumed to be in solid-body rotation so that the radial tangential wind profile inside the RMW does not change with B.

Three experiments with different initial vortex structures were conducted (Table 1). In experiments R60B10 and R60B05, the initial RMW was set to be 60 km with the parameter B set to 1.0 and 0.5, respectively. These two experiments were designed to examine the effect of the radial tangential wind profile (vortex shape) of the initial vortex on the initial spinup and the subsequent IR. Experiment R100B10 is similar to R60B10 except that the initial RMW was larger and set to be 100 km. As a result, the difference between experiments R100B10 and R60B10 reflects the sensitivity of the simulated TC to the inner-core size (RMW) of the initial vortex. The maximum tangential wind of the initial vortex was set to be 20 m s^{-1} for the standard experiment in each of the three groups. Figure 1 shows the radial profile of the tangential wind and inertial stability of the initial vortex at the lowest model level in the standard run of each experiment. We can see that the vortices in experiments R60B10 and R60B05 have the same inertial stability in the inner-core region, but the former has relatively lower inertial stability outside the RMW. In comparison with the vortex in experiment R60B10, the vortex in experiment R100B10 has much smaller inertial stability in the inner-core region, but has relatively larger inertial stability outside the RMW. Therefore, our experimental design attempts to address how sensitive the simulated TC IR is to the radial profile

Table 1. Summary of the numerical experiments performed in this study. RMW is the radius of maximum wind of the initial TC vortex and B is the radial decaying parameter of tangential wind speed outside the RMW in Eq. (1) and the mean IR (m s^{-1} day^{-1}) for maximum 10-m wind speed increased from 25 m s^{-1} to 45 m s^{-1} as given in Fig. 3.

Experiment	Initial vortex		Mean Intensification Rate (m s^{-1} day^{-1}) for maximum 10-m wind speed increased from 25 m s^{-1} to 45 m s^{-1} as given in Fig. 3	Maximum IR during intensification (m s^{-1} day^{-1})
	RMW (km)	B		
R60B10	60	1.0	28	31
R60B05	60	0.5	17	21
R100B10	100	1.0	15	18

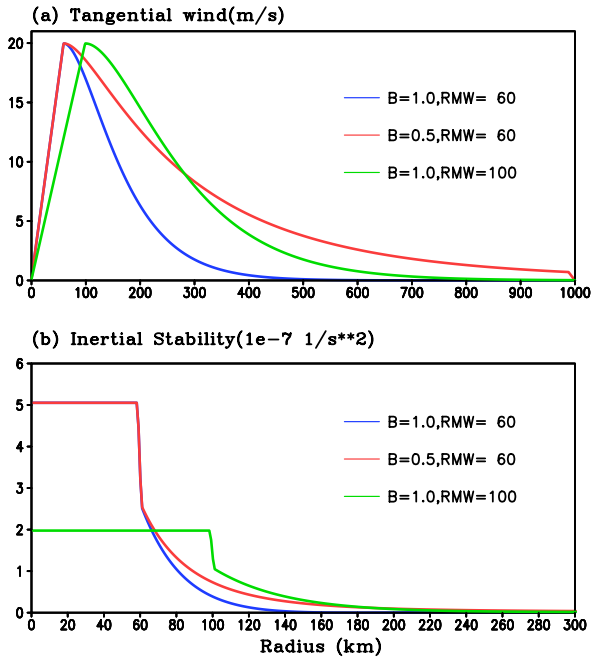

Fig. 1. Radial profiles of (a) tangential wind (m s^{-1}) and (b) inertial stability parameter of the initial vortices used in experiments R60B10, R60B05, and R100B10 (see Table 1).

of the tangential wind and thus the inertial stability in both the inner- and outer-core regions of the initial TC vortex in the simulations.

To reduce the effect of internal variability on the physical sensitivity to the initial storm structure, an ensemble of 17 runs was conducted for each experiment, with a perturbation of an increment of 0.1 m s^{-1} added to the initial maximum tangential wind speed and a perturbation of an increment of 1 km added to the initial RMW to their corresponding values in the standard run of each experiment. For example, for the ensemble members in experiment R60B10, the initial Vmax varies from 19.8 to 20.2 m s^{-1} for the RMW varying from 58 to 62 km. Similar ensemble members were constructed for both R60B05 and R100B10. A total of 51 12-day simulations were conducted for the three groups. For all simulations, the parameterization schemes and initial environmental sounding are identical to those used in Rotunno and Emanuel (1987), except the use of a double-moment microphysics scheme that includes ice processes (Morrison et al. 2009) and the horizontal mixing length of 750 m as used in Bryan (2012). The default setting for the asymptotic vertical turbulence length scale of 100 m, the surface exchange coefficient for entropy, and the surface drag coefficient for momentum suitable to TC simulations (option cecd = 3) in CM1 version 17 were used in this study. The sea surface temperature was set to be constant at 26.13°C.

3. Results

3.1 Storm intensity evolution

Figure 2 shows the time evolution of storm intensity in terms of the maximum 10-m wind speed (V_{max}) and the central sea-level pressure from all of the ensemble members (thin lines) and the ensemble mean (thick lines) for each experiment. We can see that large variability among ensemble members exists in all three experiments. The variability is the largest for the initially larger vortex in experiment R100B10. Nevertheless, the difference between the three ensemble means is generally larger than the variability among the ensemble members in each experiment, both in the intensification phase and in the mature phase. Thus, the difference among the three experiments in terms of their ensemble means is meaningful and reflects a physical sensitivity rather than internal variability. Therefore, in the following discussion, we will mainly focus on the ensemble means for the three experiments and their differences in the initial spinup and the subsequent primary intensification periods. Herein, the initial spinup period (with IR less than 2.5 m s^{-1} day^{-1}) is defined as the period before the beginning of the primary intensification (with IR larger than 2.5 m s^{-1} day^{-1}).

As we can see from Figs. 2 and 3, the spinup period varies significantly among the three experiments. The spinup period was shorter for the storm with the initially smaller RMW, i.e., about 24 h in both R60B10 and R60B05 compared with 54 h in R100B10. The initial spinup period seemed to be insensitive to the radial decay rate of tangential wind outside the RMW of the initial TC vortex, but very sensitive to the initial RMW (R60B10/R60B05 versus R100B10). The subsequent primary intensification period was shorter, and thus, the IR was larger for the storm with more rapidly decaying tangential wind outside the RMW and/or a smaller initial RMW, such as experiment R60B10 versus R100B10 or R60B05. After the initial spinup period, the storm in R100B10 intensified until about 168 h with a smaller IR, much longer than the storm in either R60B05 (until about 128 h) or R60B10 (108 h). A similar feature can be seen in the evolution of central sea-level pressure (Fig. 2b). Note that, during the mature stage in the three experiments, the ensemble-mean maximum intensities of the simulated TCs

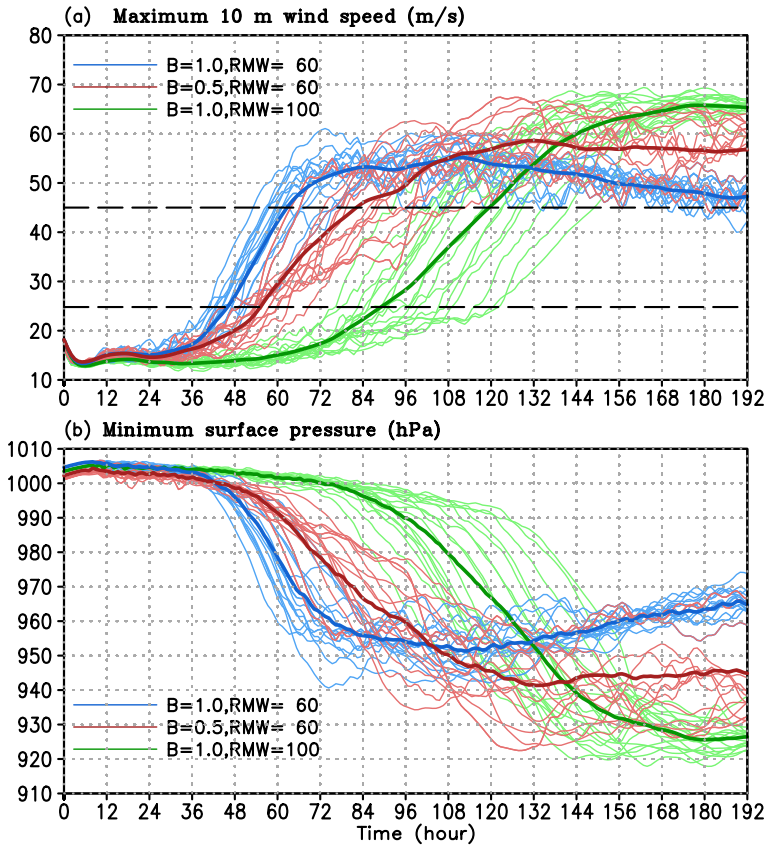

Fig. 2. Time evolutions of maximum 10-m wind speed (m s^{-1}) and minimum central sea level pressure (hPa) in experiments R60B10 (blue), R60B05 (red), and R100B10 (green). Shown are results for all individual runs (thin) and their ensemble mean (thick) for each experiment. The two dashed horizontal lines indicate storm intensity between 25 m s^{-1} and 45 m s^{-1}, helping identify the starting and ending times of the RI period for the three experiments (see text for more details).

are different; those in R60B10 are particularly weaker than those in either R60B05 or R100B10 (Fig. 2a). Although the current MPI theories (Emanuel 1995, 1997) do not include any explicit storm size parameters, the results here suggest that the mature TC intensity might also depend on the initial TC inner-core size and outer-core tangential wind structure, which is a topic that needs further investigation.

To further evaluate the IR of TCs with different initial structures in the three experiments, we calculated the IR for each ensemble mean. The IR is often defined as the increase in maximum 10-m wind speed or the drop in central sea-level pressure in a given time period, often 24 h in previous observational studies (e.g., Holliday and Thompson 1979; Kaplan and DeMaria 2003; Xu and Wang 2015). Here the IR was calculated based on the intensity change in the following 6 h, and then, the value was converted to the equivalent IR in 24 h. As we can see from Fig. 3, the storm in R60B10 showed a significantly larger IR than those in R60B05 and R100B10, with the largest IRs reaching 31 m s^{-1} day^{-1} compared with about 20 m s^{-1} day^{-1} in both R60B05 and R100B10 (Fig. 3a, Table 1). Note that TCs with a broader outer tangential-wind profile or larger initial inner-core size not only have smaller IRs but also take longer time to reach their maximum IRs (Fig. 3a). The maximum IR in R100B10 occurred after about 114 h of integration, compared with 72 h in R60B05 and 57 h in R60B10.

Furthermore, if we define RI as a maximum wind-speed increase of 15 m s^{-1} in 24 h (Kaplan and DeMaria 2003; Kaplan et al. 2010), we find that the storms in R60B10 showed a shorter RI period but larger IR than in R100B10 (with the RI period lasting

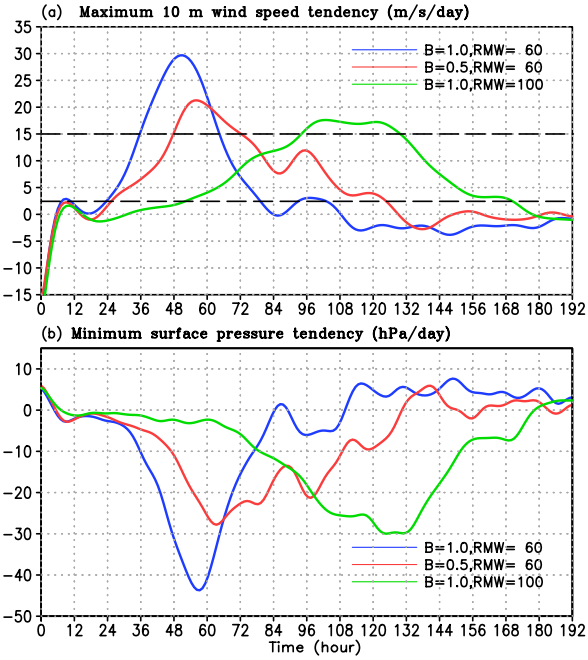

Fig. 3. Time evolutions of the ensemble mean (a) time tendency of maximum 10-m wind speed (m s^{-1} d^{-1}) and (b) time tendency of minimum central sea level pressure (hPa d^{-1}) in experiments R60B10 (blue), R60B05 (red), and R100B10 (green). The two dashed horizontal lines indicate storm intensity tendency between 2.5 m s^{-1} d^{-1} and 15 m s^{-1} d^{-1}, helping identify the starting and ending times of the RI period for the three experiments (see text for more details).

for about 26 h compared with 38 h; Fig. 3). Note that, although the duration of the RI period in R60B05 was similar to that in R60B10, the maximum IR was considerably smaller in the former than in the latter during the RI period. The present results thus indicate that TCs with more rapidly decaying tangential wind outside the RMW would intensify more rapidly, with a similar RI period if the initial RMW is similar, and TCs with a smaller initial RMW would intensify more rapidly but with a shorter duration of the RI period. This strongly suggests that the TC IR is significantly affected by both the initial vortex size and shape. In the following discussions, we will focus on both the initial spinup period and the subsequent primary intensification (or RI) period.

3.2 The initial spinup

Rotunno and Emanuel (1987, their Fig. 1) and Emanuel (1989, his Fig. 9) showed that smaller initial vortices experienced a relatively larger IR during their primary intensification period, but they did not focus on the difference in the longevity of the initial spinup period. This is mainly because the transient intensity change in the former study was too noisy, and in the latter study, convective parameterization was used and thus showed no significant differences in the duration of the initial spinup period. In our simulations, the initial spinup period shows a strong dependence on the initial TC structure, particularly the initial RMW, namely, the large difference between R60B10 and R100B10 as shown in Fig. 2a. Previous studies suggested that such an initial spinup was due to the moistening of the air column by small-scale convection in the inner-core region (Rotunno and Emanuel 1987; Emanuel 1989). This motivated us first to examine the time evolution of relative humidity (RH) in the inner-core region of the simulated TCs.

Figure 4 shows the time evolution of RH and condensational heating averaged within 1.5 times the RMW in all three experiments. The inner core was moistened continuously in the initial spinup period, but net heating is small because of evaporative cooling; the primary intensification did not begin until the column from the surface to 6 km height attained an RH over 80 %, consistent with previous studies (Bister and Emanuel 1997; Nolan 2007). This suggests that a deep moist layer in the inner-core region in the middle and lower troposphere is key to the initial spinup period of the TC (Emanuel 1989, 1995; Nolan 2007). It took about 24 h for the vortices in both R60B10 and R60B05 to become moistened in the inner-core region from the surface up to about 8 km height (Figs. 4a, b). In sharp contrast, it took about 56 h for the vortex in R100B10 to complete this initial moistening stage (Fig. 4c). This suggests that the radial profile of the initial tangential wind speed outside the RMW affects the longevity of the initial spinup period very marginally, and the initial RMW has a more significant effect on it. Nevertheless, the results demonstrate that the moistening in the inner-core region is generally faster, and thus, the initial spinup period is shorter in the initially small vortex than in the initially large vortex.

The above results can be understood in two aspects. On one hand, the initially small vortex has much large vorticity inside the RMW (Fig. 1b) and thus larger Ekman pumping in response to surface friction, which is proportional to the vertical vorticity at the top of the boundary layer (Eliassen 1971; Eliassen and Lystad

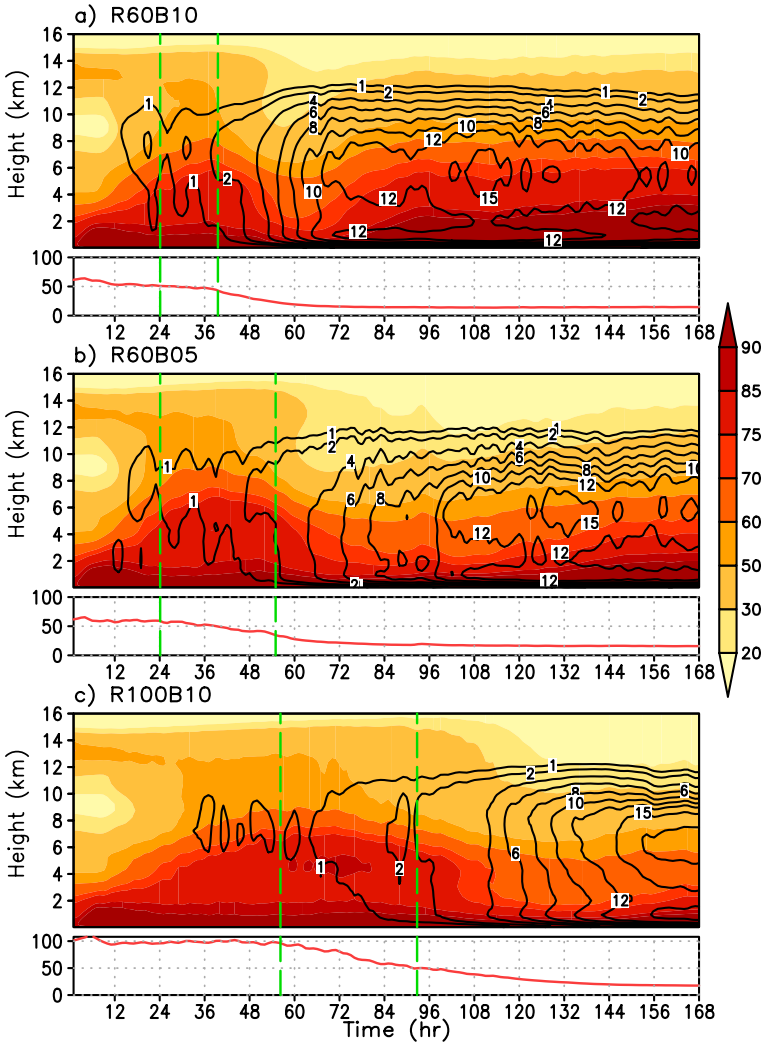

Fig. 4. Time-height cross-sections of relative humidity (%, shading) and the diabatic heating rate (K d^{-1}, contours) both averaged within the radius of 1.5 times RMW, together with the time evolution of the RMW shown at the bottom of each panel (red line). Shown are ensemble mean in experiments (a) R60B10, (b) R60B05, and (c) R100B10. The vertical line in each panel shows the time when the initial spin up period ends (left) while the primary intensification starts (right) in the corresponding experiment.

1977; Emanuel 1989). This can be seen from the vertical motion averaged in the first 3 h of simulations shown in Fig. 5. Even though it is weak and only obvious below about 2 km height, the Ekman pumping still plays an important role in transporting moisture from the surface layer upward across the boundary layer, contributing to the bottom–up moistening of the inner core of the vortex (Fig. 5). On the other hand, a TC vortex with a smaller RMW has a smaller volume in the inner core, and thus, the column of the inner core requires shorter time to moisten. Therefore, both the relatively stronger Ekman pumping and smaller inner-core volume in the initially smaller vortex contribute to the faster moistening of the inner-core column and thus shorter initial spinup period.

The moistened column in the inner core is necessary for the initiation of organized eyewall convection (Emanuel 1989). Condensational heating in eyewall convection has been viewed as "driving" the secondary circulation and spinning up the tangential wind (Schubert and Hack 1982). Condensational heating still occurred in the initial spinup period but was quite

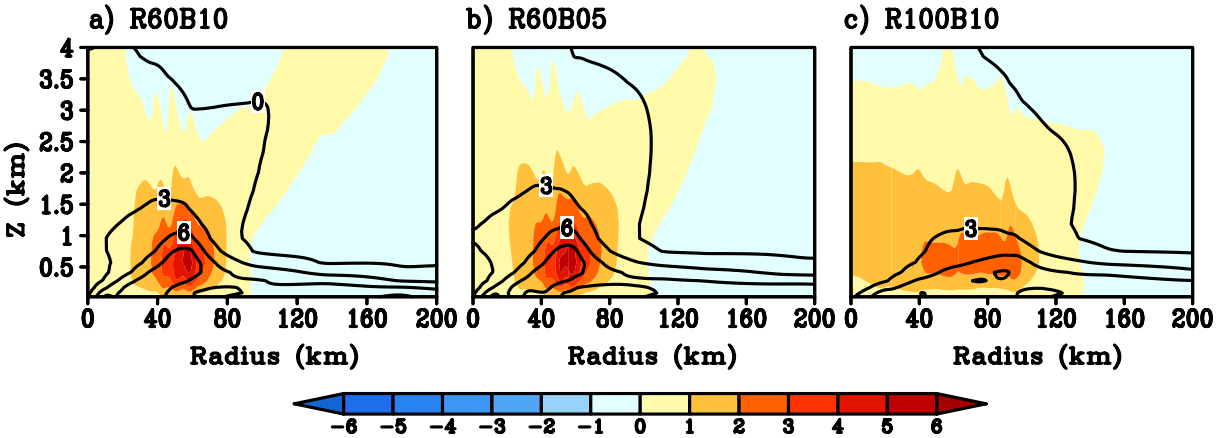

Fig. 5. Radial-vertical cross sections of vertical velocity averaged over the first 3 h simulation (shading, mm s^{-1}) and change in water vapor mixing ratio (contours, 10^{-4} kg kg^{-1}) in the first 3 h simulation in R60B10 (a), R60B05 (b), and R100B05 (c), respectively.

weak (Fig. 4) because of the small area coverage of deep convection in the inner-core region and the strong downdrafts. Weak diabatic heating appeared much earlier in both R60B10 and R60B05 than in R100B10, which was consistent with the slower moistening and the longer initial spinup period in the latter than in the former. Note that the RMW at the lowest model level changed little during this moistening and initial spinup period in all three experiments, indicating that the boundary-layer inflow did not become well organized until the end of the initial spinup period (not shown). Therefore, the initial spinup of the TC vortices in the model simulations can be considered as a moistening process of the inner-core region during which first the Ekman pumping and later the loosely organized deep convection gradually moistened the inner-core column from bottom up.

The activity of convection in response to the moistening can be inferred from the evolution of precipitation as shown in Fig. 6. Precipitation (and convection) initially appeared near the RMW in all three experiments and propagated radially outward (Fig. 6), particularly for the vortex with initially larger RMW in R100B10 (Fig. 6c) or the vortex with relatively slower radial decay of tangential wind outside the RMW in R60B05 (Fig. 6b). This seems to suggest that larger winds outside the RMW (or in the initially larger vortex) contribute to larger surface moisture flux (Fig. 6) and thus favor more convection to develop outside the RMW, which is consistent with the finding in Xu and Wang (2010a, b). As a result, the initially smaller vortex with a rapid radial decay of the tangential wind outside the RMW in R60B10 showed an earlier organization of convection (and precipitation) and thus an earlier onset of the subsequent primary intensification than in either R60B05 or R100B10.

The moistening and heating in the inner-core region were also reflected in the time evolution of the temperature anomaly averaged within the RMW and the equivalent potential temperature (θ_e) averaged between the RMW and 1.5 times the RMW in each experiment (Fig. 7). The temperature anomaly here was defined as the temperature difference from the initial state. During the initial spinup period, after about 12 h of integration, weak warm anomalies appeared in the middle to upper troposphere centered at around 8–10 km height, and weak cold anomalies occurred in the lower troposphere at about 4 km height in all experiments. The cold anomalies were not only associated with melting and evaporation of cloud condensates but also with sublimation cooling as pointed out by Zhang et al. (2002) and Sawada and Iwasaki (2007) because of the unsaturated environment in the inner-core region. Consistent with the slower moistening of the air column in the inner-core region in R100B10 than in either R60B10 or R60B05, the low-level cold anomalies persisted much longer in R100B10 (Fig. 7c). The gradual moistening of the inner-core column was also consistent with the gradual increase in low-level θ_e averaged in the annulus between the RMW and 1.5 RMW. The initial low θ_e between 2 and 8 km reflected a convectively unstable state. The low-level θe started to increase after the initiation of convection and continued increasing during the primary intensification

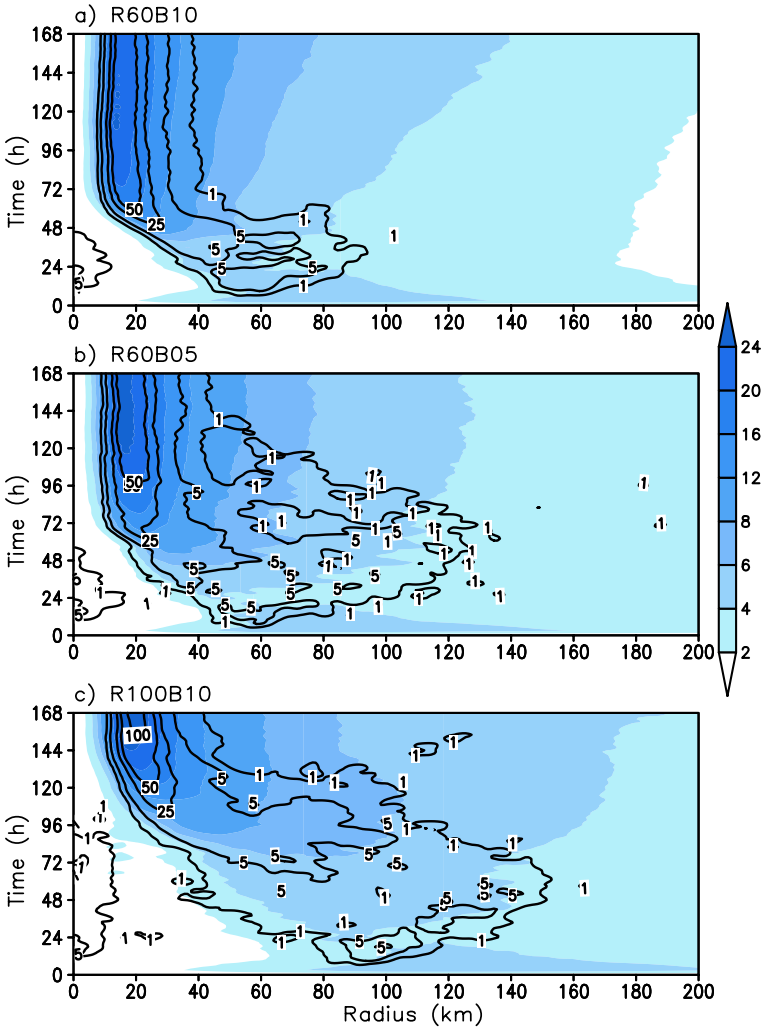

Fig. 6. Time-radius cross-sections of the surface water vapor flux (shading, 10^{-5} kg kg^{-1} m s^{-1}) and rain rate (contours, mm h^{-1}) for the ensemble mean in (a) R60B10, (b) R60B05, and (c) R100B10, respectively.

period, which was marked when a warm-core structure with positive temperature anomalies greater than 5 K was established in each experiment (Figs. 2, 7).

The above results suggest that the longevity of the initial spinup period is determined by how fast the inner-core region becomes nearly saturated in the middle and lower troposphere, and thus, deep convection near the RMW was initiated and organized. The initially larger vortex took a much longer time to moisten and saturate in the inner-core region than the initially smaller vortex and thus experienced a prolonged spinup period. These results are generally consistent with the results of Rotunno and Emanuel (1987) and Emanuel (1989, 1995). We also demonstrated that the time needed for the inner core to moisten was largely determined by the Ekman pumping and the volume of the inner-core region. As a result, it is not surprising that the longevity of the moistening of the inner core is more sensitive to the initial inner-core size (such as the RMW) of the TC vortex than to the radial decay rate of tangential wind outside the RMW. The result that an initial TC vortex with smaller RMW has a shorter spinup period is consistent with Miyamoto and Takemi (2015), but they mainly focused on dynamical aspects and proposed that a TC with a larger Rossby number (smaller RMW) tend to enter RI phase earlier (or equivalently, the spinup period is shorter).

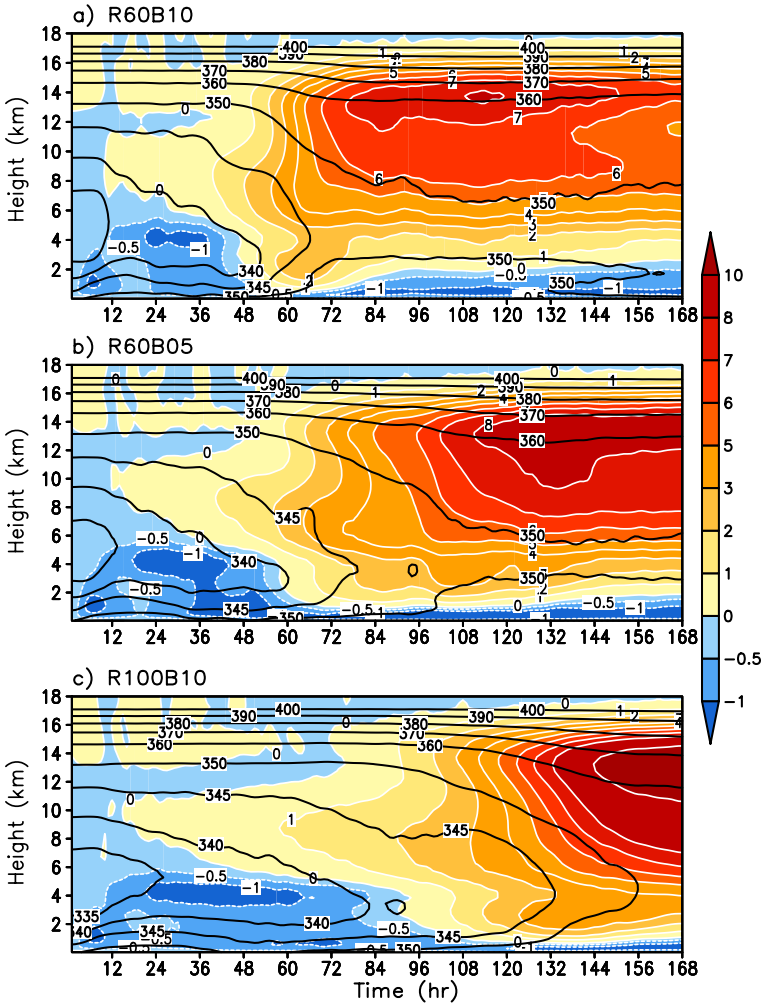

Fig. 7. Time-height cross-sections of perturbation temperature (K, shading) average within the RMW and equivalent potential temperature (K, contours) averaged between the RMW and the 1.5 times RMW of the simulated TC center for the ensemble mean in (a) R60B10, (b) R60B05, and (c) R100B10.

3.3 *The primary intensification*

After the initial spinup period, the TC vortices started their primary intensification, marked by an IR greater than 2.5 m s^{-1} day^{-1} in all three experiments (Fig. 3). Note that the primary intensification period can be classified into three stages in each experiment. In the first stage, the storm intensified slowly with IR less than 15 m s^{-1} day^{-1}, which was followed by an RI stage and then a stage with a reduced IR of less than 15 m s^{-1} day^{-1} before the storm reached a quasi-steady state (Figs. 2, 3). On the basis of Figs. 2a and 3a, we consider the RI stage as simply the increase in the 10-m maximum wind speed from 25 to 45 m s^{-1}, equivalent for a TC to intensify from a tropical storm to a category-2 hurricane, in all three experiments, as shown in horizontal dashed lines in Fig. 2a.

As discussed in Section 3a above, the IR of the simulated TC during the primary intensification period differs considerably among the three experiments. Specifically, the storm with the larger initial RMW in R100B10 intensified much more slowly than that with the smaller initial RMW in R60B10. For TCs with the same initial RMW in R60B10 and R60B05, although the TCs had similar initial spinup periods, the storm with an initially more rapid radial decay of tangential wind outside the RMW in R60B10 intensified more rapidly. Previous studies based on balanced dynamics suggest that the IR of a TC is determined by the

dynamical efficiency of eyewall heating, which is predominantly controlled by the inner-core inertial stability (Schubert and Hack 1982), and both the magnitude and the radial location of diabatic heating relative to the RMW (Vigh and Schubert 2009; Pendergrass and Willoughby 2009).

As we can see from Fig. 1, the initially smaller TC vortices in both R60B10 and R60B05 had much higher inertial stability inside the RMW, implying that they had higher dynamical efficiency in response to eyewall heating. Since condensational heating in the inner core was established and well organized much earlier in these two experiments (Fig. 4), it is not surprising that the TCs in R60B10 and R60B05 intensified more rapidly than the TC in R100B10 (Figs. 2, 3). Note that the IR in the first stage of the primary intensification period was relatively small in all experiments, which was consistent with the small diabatic heating rate in the inner-core region (Fig. 4). The RI stage began when the diabatic heating rate averaged roughly in the eyewall reached about 2 K day^{-1} in all experiments (Fig. 4). It seems to suggest that the IR was closely related to the rate of increase in diabatic heating in the eyewall and the increase in inertial stability in the inner-core region in all experiments (Figs. 3, 4). This is consistent with the prediction based on the balanced vortex model by Schubert and Hack (1982) and Pendergrass and Willoughby (2009), and the results in a full-physics real-case simulation of Typhoon Megi (2010) as investigated in Wang and Wang (2014).

As both diabatic heating and inertial stability in the inner core are functions of the storm intensity and the inner-core size, for a fair comparison, it is important to compare various parameters when the storms had similar intensities during their RI stage. For a detailed comparison, we chose the period during which the simulated TCs intensified from 25 to 45 m s^{-1} in all three experiments. Figures 8a–c show the radial distributions of tangential wind speed, inertial stability, and diabatic heating rate vertically averaged between 0.025 and 3 km height and temporally averaged in the corresponding period in each experiment. Note that, although the time average was done for the period between two given intensities, the averaged tangential winds still differed slightly among the three experiments (Fig. 8a). For the TCs with the same initial RMW in R60B10 and R60B05, the inertial stability is very similar in the inner-core region within a radius of 40 km (Fig. 8b). The TC in R60B05 shows relatively higher inertial stability and larger tangential wind speed outside the 40-km radius than in R60B10. A common feature in all three experiments was the large diabatic heating rate occurring inside the RMW (Fig. 8c), consistent with the observations for intensifying TCs (Rogers et al. 2013). However, the diabatic heating rate is higher in the inner-core region and smaller outside a radius of 80 km in R60B10 than in R60B05. This radial distribution of heating is consistent with the radial inflow averaged between 0.25 and 1 km height in the boundary layer (Fig. 8d). This indicates that the larger inertial stability outside the RMW in R60B05 (Fig. 8b) is responsible for the relatively weaker boundary-layer inflow near the RMW and relatively stronger boundary-layer inflow in the outer-core region (Fig. 8d). Both inertial stability and diabatic heating rate are considerably smaller in the inner-core region and larger outside the radius of 40 km in R100B10 than those in either R60B10 or R60B05 (Figs. 8b, c). This is consistent with the larger inflow outside the radius of 40 km and smaller inflow inside the 35-km radius in R100B10 than in R60B10 and R60B05 (Fig. 8d).

The radial distribution of inertial stability (and absolute vorticity) and the boundary-layer inflow seem to explain the different IRs among the three experiments (Fig. 3). This can be understood by conducting a tangential wind budget analysis for each of the experiments. The budget equation can be written as

$$\frac{\partial \overline{v}}{\partial t} = -\overline{u(\zeta + f)} - \overline{w\frac{\partial v}{\partial z}} + \overline{F}, \tag{2}$$

where t is time, z is the physical height, u, v are the radial and tangential wind speeds, ζ is the vertical relative vorticity, f is the Coriolis parameter, and w is the vertical velocity. The overbar signifies the ensemble and temporal mean in the period as the TC intensified from 25 to 45 m s^{-1}, marked as horizontal lines in Fig. 2a, which was chosen to reduce the intensity dependence of the budget analyses for a given RI period. Note that the budget analysis that we conducted was almost residual-free since all terms were calculated during the model time integration with the same finite-differencing schemes.

Figure 9 shows the budget results in the lowest 3 km model atmosphere based on hourly model outputs for the three experiments. As expected, the larger positive tangential wind tendency due to radial advection in the boundary layer in R60B10 than in R100B10 is due to the stronger radial inflow, which is consistent with the higher absolute vorticity above the boundary layer (Fig. 8d). The negative tangential wind tendency immediately above the inflow boundary layer was

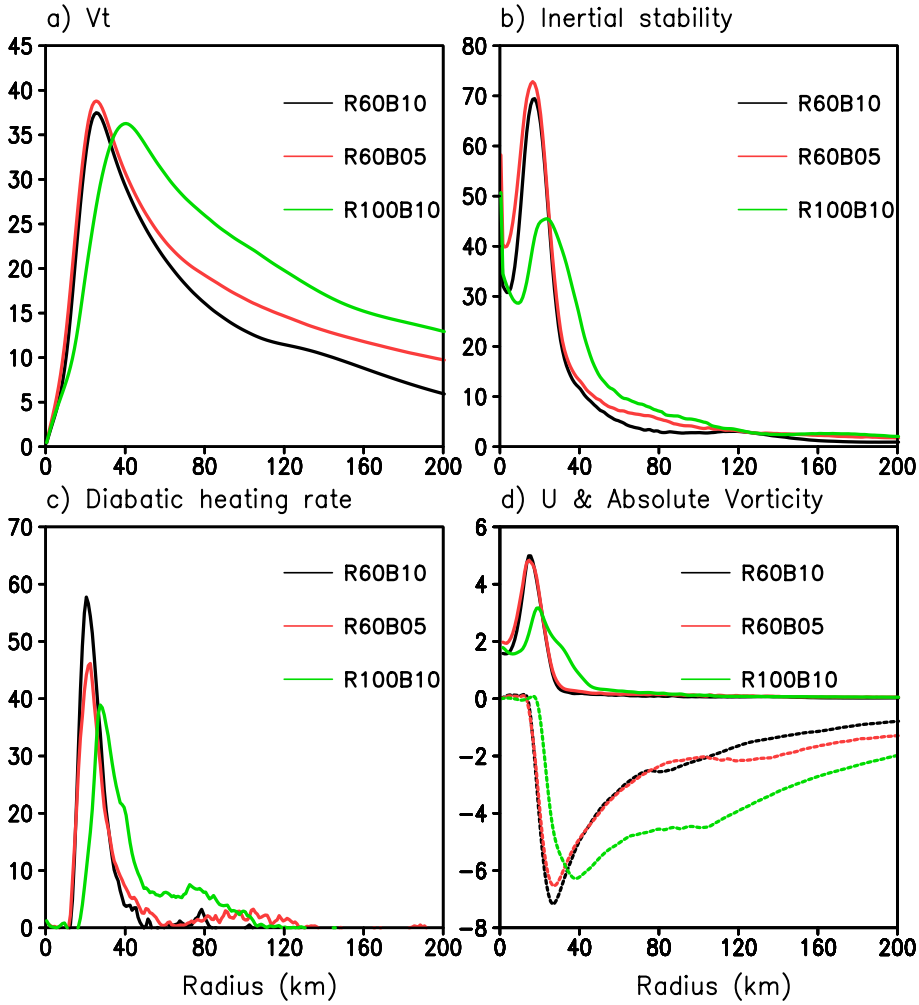

Fig. 8. The radial distributions of a) the tangential wind (m s^{-1}), b) normalized inertial stability parameter I by Coriolis parameter, c) diabatic heating rate (K h^{-1}), averaged between 25 m and 3 km heights, and (d) radial wind (m s^{-1}, dash) and vertical absolute vorticity (10^{-3} s^{-1}, solid) averaged between 25 m and 1 km heights in R60B10 (black), R60B05 (red), and R100B10 (green). All variables are averaged over the RI period as the storm intensified from 25 m s^{-1} to 45 m s^{-1} in each experiment (see Fig. 2).

related to the radial outflow, which was larger in R60B10 as well, and was largely offset (but accounts for $\partial v/\partial t > 0$ above the boundary layer) by the vertical advection (third row). The diffusion term is negative and significant in the boundary layer, particularly in regions with high tangential wind speeds near the RMW in all experiments. The net tangential wind tendency, namely, the local tangential wind tendency, is the largest in R60B10, followed by R60B05 and then R100B10 (top row in Fig. 9). This is consistent with the different IRs shown in Fig. 3. Therefore, the tangential wind budget results demonstrate that the largest IR in R60B10 among the three experiments is primarily due to the stronger inflow in the boundary layer which brings higher absolute angular momentum inward into the inner-core region and then transported upward in the eyewall. This process is enhanced by higher inertial stability (absolute vorticity) near the RMW and weaker inertial stability outside the RMW in R60B10 compared to that in either R60B05 or R100B10. As a result, a stronger positive feedback exists between the boundary-layer inflow and diabatic heating in the eyewall in R60B10. This is consistent with the intensification mechanism elaborated based

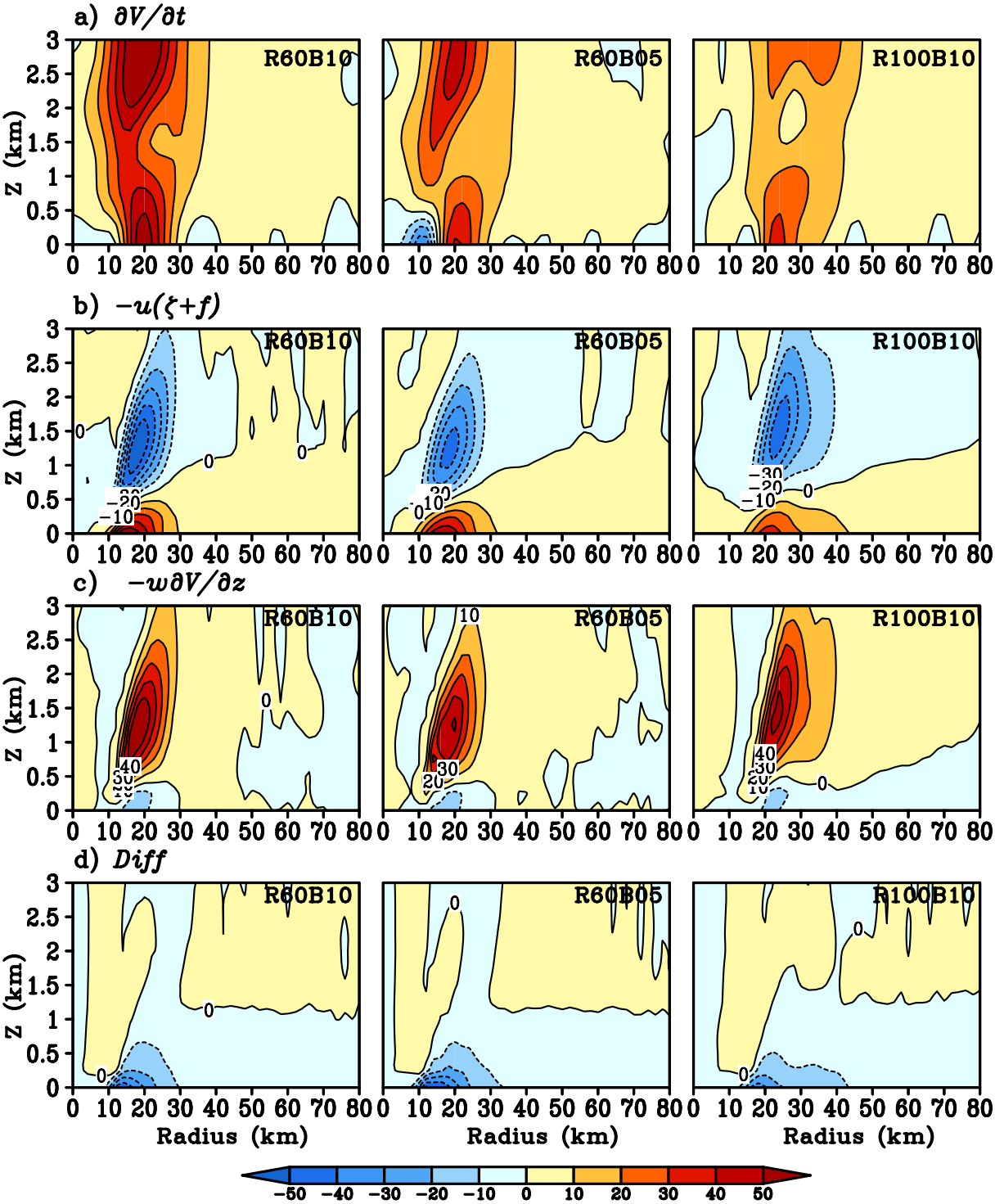

Fig. 9. Tangential wind budget averaged during the RI period in experiments, respectively, R60B10 (left column), R60B05 (central column), and R100B10 (right column) for (a) the local change of tangential wind (m s^{-1} day^{-1}), (b) the radial advection term $[-u(\zeta + f)]$, (c) the vertical advection term, and (d) the horizontal and vertical diffusion term including surface friction. Note that all terms on the right hand side in Eq. (2) are in m s^{-1} hr^{-1}.

on results from a full-physics real-case simulation of Typhoon Megi (2010) by Wang and Wang (2014) and implications from balanced dynamics (Schubert and Hack 1982; Pendergrass and Willoughby 2009).

Several other points should be mentioned here. First, although diabatic heating in eyewall convection is the key to the intensification of a TC, the IR during RI in the simulations (Fig. 3a) was not determined by the diabatic heating rate in the eyewall in all simulations but by the increasing tendency of the diabatic heating rate (contours in Fig. 4). Second, the drying period with the reduced inner-core RH in each experiment (shading in Fig. 4) coincided with the end of the RI phase, which indicates the strong subsidence in the eye region associated with the RI phase (not shown). Third, there were two cores of maximum temperature anomalies in the simulated TCs in all three experiments during the RI period (Fig. 7): one was centered in the middle troposphere around 7 km height, and the other was located in the upper troposphere near 14 km height. Note that the double warm-core structure mainly occurred in the RI period, the middle-level warm core was dominant in the pre-RI stage, and the upper-level warm core was dominant after the RI period. The present experiments indicate that the warm core appeared in the middle troposphere in the early weak stage of the simulated TCs. In contrast, the upper-level warm core formed and intensified as the TC intensified and the middle-level warm core lowered. Eventually, the upper-level warm core dominated the middle-level warm core when the storm became intense, displaying a single warm-core structure (Fig. 7). Note that the double warm-core structure during the RI phase was more evident in the initially larger storm and in the storm with a more broad outer tangential wind in R100B10 and R60B05 than in the initially smaller and more compact storm in R60B10. Our results are, in general, consistent with some recent studies that have also documented double warm-core structure in intensifying TCs (Stern and Nolan 2012; Wang and Wang 2014; Stern and Zhang 2013; Kieu et al. 2016; Ohno and Satoh 2015).

4. Conclusions

In this study, the dependence of TC IR on its initial vortex structure has been examined based on ensemble simulations using the nonhydrostatic axisymmetric cloud-resolving model CM1 of Bryan and Fritsch (2002). Three simulations, each including 17 ensemble runs, were performed and analyzed. The model was initialized with TC vortices of different initial RMWs (60 km versus 100 km) and different radial decay rates of tangential wind outside the RMW (decay parameter B of 1.0 versus 0.5). The analyses have been focused on both the longevity of the initial spinup period (with the IR less than 2.5 m s^{-1} day^{-1}) and the subsequent primary intensification period.

The results showed that the longevity of the initial spinup period was largely determined by the time needed for the inner-core region to become nearly saturated in the middle and lower troposphere so that deep convection near the RMW could be initiated and organized. As a result, the initially larger TC vortex, which contained a larger volume of dry air mass inside the RMW and had weaker Ekman pumping in the inner core, took a relatively longer time to become saturated and thus experienced a longer initial spinup period. The IR during the subsequent primary intensification period was largely controlled by the inertial stability in both the inner- and outer-core regions and the initial size of the TC vortex. The initially smaller vortex, which had higher inertial stability inside the RMW, developed stronger boundary-layer inflow near the RMW, favoring a larger inward transport of absolute angular momentum (AAM) in the lower troposphere and thus higher IR. The vortex initially with the more rapid radial decay of tangential wind outside the RMW, which had relatively lower inertial stability outside the RMW, developed weaker boundary-layer inflow in the outer-core region, favoring a larger inward transport of AAM and thus higher IR. In addition, the storm with an initially large RMW or with a slow radial decay of tangential wind outside the RMW also developed active convection outside the eyewall. Diabatic heating in the outer-core region contributed to the growth of the storm size and reduced the IR of the simulated storm, as previously demonstrated by Wang (2009). These results are, in general, consistent with recent observational studies for North Atlantic TCs based on airborne-radar data (Rogers et al. 2013) and the best track TC data (Carrasco et al. 2014; Xu and Wang 2015).

Therefore, the results from this study, together with those of Rogers et al. (2013), Carrasco et al. (2014), and Xu and Wang (2015), strongly suggest that the vortex structure needs to be reasonably estimated from observations and accurately initialized in numerical weather prediction models used for real-time TC forecasts. Although the RMW is currently estimated routinely in various ocean basins, the radial tangential wind profile, however, has not been routinely provided in real time in any ocean basin (Chavas and Emanuel 2010; Knaff et al. 2011; Elsberry et al. 2013). Efforts toward the accurate estimation of the TC structure

based on observations could lead to improved TC initialization and thus accuracy of TC intensity forecasts by numerical models.

Acknowledgments

The authors are grateful to Drs. Richard Rotunno and George Bryan for their helpful discussions and constructive comments/suggestions on an earlier version of the manuscript. This study has been supported in part by the National Basic Research and Development Project (973 program) of China under contract no. 2015CB452805 and in part by National Natural Science Foundation of China under grants 41675044, 41130964 and 41375068 and NSF grant AGS-1326524, Special Fund for Meteorological Scientific Research in the Public Interest (Grant No. GYHY 201406006), and Basic Research Fund of CAMS 2016 Z003. Almost all of the figures were produced using the Grid Analysis and Display System (GrADS).

References

Bister, M., and K. A. Emanuel, 1997: The genesis of Hurricane Guillermo: TEXMEX analyses and a modeling study. *Mon. Wea. Rev.*, **125**, 2662–2682.

Bryan, G. H., 2012: Effects of surface exchange coefficients and turbulence length scales on the intensity and structure of numerically simulated hurricanes. *Mon. Wea. Rev.*, **140**, 1125–1143.

Bryan, G. H., and J. M. Fritsch, 2002: A benchmark simulation for moist nonhydrostatic numerical models. *Mon. Wea. Rev.*, **130**, 2917–2928.

Bryan, G. H., and R. Rotunno, 2009a: Evaluation of an analytical model for the maximum intensity of tropical cyclones. *J. Atmos. Sci.*, **66**, 3042–3060.

Bryan, G. H., and R. Rotunno, 2009b: The maximum intensity of tropical cyclones in axisymmetric numerical model simulations. *Mon. Wea. Rev.*, **137**, 1770–1789.

Carrasco, C. A., C. W. Landsea, and Y.-L. Lin, 2014: The influence of tropical cyclone size on its intensification. *Wea. Forecasting*, **29**, 582–590.

Chavas, D. R., and K. A. Emanuel, 2010: A QuikSCAT climatology of tropical cyclone size. *Geophys. Res. Lett.*, **37**, L18816, doi:10.1029/2010GL044558.

Chen, H., D.-L. Zhang, J. Carton, and R. Atlas, 2011: On the rapid intensification of Hurricane Wilma (2005). Part I: Model prediction and structural changes. *Wea. Forecasting*, **26**, 885–901.

Eliassen, A., 1971: On the Ekman layer in a circular vortex. *J. Meteor. Soc. Japan*, **49**, 784–789.

Eliassen, A., and M. Lystad, 1977: The Ekman layer of a circular vortex: A numerical and theoretical study. *Geophys. Norv.*, **31**, 1–16.

Elsberry, R. L., L. Chen, J. Davidson, R. Rogers, Y. Wang, and L. Wu, 2013: Advances in understanding and forecasting rapidly changing phenomena in tropical cyclones. *Trop. Cyclone Res. Rev.*, **2**, 13–24.

Emanuel, K. A., 1989: The finite-amplitude nature of tropical cyclogenesis. *J. Atmos. Sci.*, **46**, 3431–3456.

Emanuel, K. A., 1995: The behavior of a simple hurricane model using a convective scheme based on subcloud-layer entropy equilibrium. *J. Atmos. Sci.*, **52**, 3960–3968.

Emanuel, K. A., 1997: Some aspects of hurricane inner-core dynamics and energetics. *J. Atmos. Sci.*, **54**, 1014–1026.

Hill, K. A., and G. M. Lackmann, 2009: Influence of environmental humidity on tropical cyclone size. *Mon. Wea. Rev.*, **137**, 3294–3315.

Holliday, C. R., and A. H. Thompson, 1979: Climatological characteristics of rapidly intensifying typhoons. *Mon. Wea. Rev.*, **107**, 1022–1034.

Kaplan, J., and M. DeMaria, 2003: Large-scale characteristics of rapidly intensifying tropical cyclones in the North Atlantic basin. *Wea. Forecasting*, **18**, 1093–1108.

Kaplan, J., M. DeMaria, and J. A. Knaff, 2010: A revised tropical cyclone rapid intensification index for the Atlantic and eastern North Pacific basins. *Wea. Forecasting*, **25**, 220–241.

Kieu, C., V. Tallapragada, D.-L. Zhang, and Z. Moon, 2016: On the development of double warm-core structures in intense tropical cyclones. *J. Atmos. Sci.*, **73**, 4487–4506.

Knaff, J. A., S. A. Seseske, M. DeMaria, and J. L. Demuth, 2004: On the influences of vertical wind shear on symmetric tropical cyclone structure derived from AMSU. *Mon. Wea. Rev.*, **132**, 2503–2510.

Knaff, J. A., M. DeMaria, D. A. Molenar, C. R. Sampson, and M. G. Seybold, 2011: An automated, objective, multiple-satellite-platform tropical cyclone surface wind analysis. *J. Appl. Meteor. Climatol.*, **50**, 2149–2166.

Merrill, R. T., 1984: A comparison of large and small tropical cyclones. *Mon. Wea. Rev.*, **112**, 1408–1418.

Miyamoto, Y., and T. Takemi, 2015: A triggering mechanism for rapid intensification of tropical cyclones. *J. Atmos. Sci.*, **72**, 2666–2681.

Morrison, H., G. Thompson, and V. Tatarskii, 2009: Impact of cloud microphysics on the development of trailing stratiform precipitation in a simulated squall line: Comparison of one- and two-moment schemes. *Mon. Wea. Rev.*, **137**, 991–1007.

Nolan, D. S., 2007: What is the trigger for tropical cyclogenesis? *Aust. Meteor. Mag.*, **56**, 241–266.

Ohno, T., and M. Satoh, 2015: On the warm core of a tropical cyclone formed near the tropopause. *J. Atmos. Sci.*, **72**, 551–571.

Pendergrass, A. G., and H. E. Willoughby, 2009: Diabatically induced secondary flows in tropical cyclones. Part I: Quasi-steady forcing. *Mon. Wea. Rev.*, **137**, 805–821.

Rogers, R., 2010: Convective-scale structure and evolution during a high-resolution simulation of tropical cyclone rapid intensification. *J. Atmos. Sci.*, **67**, 44–70.

Rogers, R., P. Reasor, and S. Lorsolo, 2013: Airborne doppler observations of the inner-core structural differences between intensifying and steady-state tropical cyclones. *Mon. Wea. Rev.*, **141**, 2970–2991.

Rotunno, R., and K. A. Emanuel, 1987: An air–sea interaction theory for tropical cyclones. Part II: Evolutionary study using a nonhydrostatic axisymmetric numerical model. *J. Atmos. Sci.*, **44**, 542–561.

Sawada, M., and T. Iwasaki, 2007: Impacts of ice phase processes on tropical cyclone development. *J. Meteor. Soc. Japan*, **85**, 479–494.

Schubert, W. H., and J. J. Hack, 1982: Inertial stability and tropical cyclone development. *J. Atmos. Sci.*, **39**, 1687–1697.

Stern, D. P., and D. S. Nolan, 2012: On the height of the warm core in tropical cyclones. *J. Atmos. Sci.*, **69**, 1657–1680.

Stern, D. P., and F. Zhang, 2013: How does the eye warm? Part I: A potential temperature budget analysis of an idealized tropical cyclone. *J. Atmos. Sci.*, **70**, 73–90.

Vigh, J. L., and W. H. Schubert, 2009: Rapid development of the tropical cyclone warm core. *J. Atmos. Sci.*, **66**, 3335–3350.

Wang, H., and Y. Wang, 2014: A numerical study of Typhoon Megi (2010). Part I: Rapid intensification. *Mon. Wea. Rev.*, **142**, 29–48.

Wang, Y., 2009: How do outer spiral rainbands affect tropical cyclone structure and intensity? *J. Atmos. Sci.*, **66**, 1250–1273.

Wang, Y., and C.-C. Wu, 2004: Current understanding of tropical cyclone structure and intensity changes—A review. *Meteor. Atmos. Phys.*, **87**, 257–278.

Wang, Y., and J. Xu, 2010: Energy production, frictional dissipation, and maximum intensity of a numerically simulated tropical cyclone. *J. Atmos. Sci.*, **67**, 97–116.

Weatherford, C. L., and W. M. Gray, 1988: Typhoon structure as revealed by aircraft reconnaissance. Part I: Data analysis and climatology. *Mon. Wea. Rev.*, **116**, 1032–1043.

Xu, J., and Y. Wang, 2010a: Sensitivity of the simulated tropical cyclone inner-core size to the initial vortex size. *Mon. Wea. Rev.*, **138**, 4135–4157.

Xu, J., and Y. Wang, 2010b: Sensitivity of tropical cyclone inner core size and intensity to the radial distribution of surface entropy flux. *J. Atmos. Sci.*, **67**, 1831–1852.

Xu, J., and Y. Wang, 2015: A statistical analysis on the dependence of tropical cyclone intensification rate on the storm intensity and size in the North Atlantic. *Wea. Forecasting*, **30**, 692–701.

Zhang, D.-L., Y. Liu, and M. K. Yau, 2002: A multiscale numerical study of Hurricane Andrew (1992). Part V: Inner-core thermodynamics. *Mon. Wea. Rev.*, **130**, 2745–2763.